

## Capillary film and breakup mechanism in the squeezing to dripping transition regime at the mesoscale between micro and milli-fluidics

V. M. Freytes, M. Rosen, and A. D'Onofrio

Citation: *Chaos* **28**, 103104 (2018); doi: 10.1063/1.5033451

View online: <https://doi.org/10.1063/1.5033451>

View Table of Contents: <http://aip.scitation.org/toc/cha/28/10>

Published by the [American Institute of Physics](#)

---

---



**Chaos**  
An Interdisciplinary Journal of Nonlinear Science

**Fast Track Your Research. *Submit Today!***

## Capillary film and breakup mechanism in the squeezing to dripping transition regime at the mesoscale between micro and milli-fluidics

V. M. Freytes, M. Rosen, and A. D'Onofrio

*Grupo de Medios Porosos—Facultad de Ingeniería, Universidad de Buenos Aires-CONICET, Av. Paseo Colón 850, C1063ACV Ciudad Autónoma de Buenos Aires, Argentina*

(Received 5 April 2018; accepted 21 September 2018; published online 9 October 2018)

We report a study of droplet generation in two phase flows of non-miscible fluids in a T-shaped array of circular channels, at the mesoscale between micro- and milli-fluidics. Our experiments show that the balance between the different types of forces (capillary forces, shear viscous forces, etc.) may differ significantly from that found by previous authors in smaller, microfluidics channels. The results may, therefore, be applied to practical systems in which droplets act as small chemical reactors or help enhance mixing. We suggest a possible interesting extension to the generation of drops inside porous media. We report experiments in which the length of the droplets and the residual thickness of the surrounding fluid film are systematically measured as a function of the respective flow rates of the two fluids: These results are carefully compared to theoretical models taking into account in different ways the capillary and viscous effects and to results obtained by other authors for smaller channels. Several dimensionless control variables are tested (capillary number, ratio of the flow rates of the two fluids, etc.). Capillary film thickness is shown to be a useful variable to identify the different regimes of formation. Testing of the theoretical models with the experimental data showed that the change from one formation regime to the other is accompanied by a change in the role of viscous effects. Two models of breakup mechanisms were tested: on the one hand, the pressure buildup mechanism and, on the other hand, a second mechanism corresponds to the balance of tangential shear stresses and interfacial tension. According to the formation regimes, both models have provided satisfactory predictions of the experimental results. However, at this mesoscale, the experimental data were better described by the models dependent on the capillary number, as previously reported in systems with a low degree of confinement. *Published by AIP Publishing.* <https://doi.org/10.1063/1.5033451>

**Nowadays, microfluidics is the basis of many biotechnological developments, simply because biological samples are in a liquid state and biological organisms live in an aqueous environment. Compared to conventional techniques, the use of microdevices has many advantages: the volumes of sample and reagents are significantly reduced, which diminishes the cost of the process, and the results (diagnostic) or the products (biochemistry) are obtained in much shorter times, which is also necessary for medical emergency reasons or portability.**

**In porous media, microfluidic techniques allow for detailed studies of the flow at the confluence of channels within the media. The studies include the possible formation of drops at the micro- and mesoscale with effects on higher scales. The formation of droplets within the porous medium modifies the mixture of different solutions, increases the efficiency of chemical reactions, etc.**

**The study of capillary film and breakup mechanisms in the squeezing to dripping transition regime is proposed. The capillary film is the wetting film that surrounds the trapped droplets inside the cylindrical capillary tubes. These capillary tubes simulate the channel network in a porous medium. The breakup mechanism is the process responsible for drop formation in the convergence of two streams of fluids at the intersection of two channels.**

### I. INTRODUCTION

The main objective of this work is to achieve a better understanding of the transport of fluids in porous media formed by channels at the micro- and mesoscale. There are many works studying the effect on transport of fluids in porous media of such phenomena as local viscosity variations,<sup>1,2</sup> pattern formation by hydrodynamic instabilities,<sup>3–8</sup> chemical reactions on the contact surface of different fluids,<sup>9–17</sup> porosity variations,<sup>18</sup> and formation of precipitates.<sup>19,20</sup> Most of these studies are carried out in Hele-Shaw cells, which facilitate the observation of the phenomena in the laboratory, but leaves aside the characteristics of the porous media such as their porosity and tortuosity. For that reason, microdevices are a good tool to carry out local studies of transport processes within porous media. The microdevices allow a direct visualization and study of the phenomena in zones such as channel bifurcation or zones with sudden variations of the pore diameter in which strong flow variations are produced. These variations modify the mixing conditions of different substances and, under certain conditions, the formation of droplets and microdroplets could become an important phenomenon to consider. For this reason, we are interested in a systematic study to a better understanding of the behaviors observed at meso- and macroscales, such as those in porous media. From this point of view, it is very useful to carry out the study of droplet formation at mesoscales in the intersection

of the microscale and the milliscale (scale length ranging from  $500\ \mu\text{m}$  to  $1\ \text{mm}$ ), by clarifying the role of the different control parameters and the progression of their behavior from the microscale (scale length  $<500\ \mu\text{m}$ ) to the macroscale (scale length  $>1\ \text{mm}$ ).

In the development of microfluidics from the late 1990s, different droplet-based microfluidic platforms have been developed. In this approach, all molecular processes are confined to the volume of a single drop, allowing for even stronger reductions in reagent volume and reaction time. A second advantage of using droplets is that the contact with solid walls is eliminated. This strongly reduces problems related to the adsorption of dissolved components on the channel walls and increases the efficiency of chemical reactions. On the other hand, as far as the porous media are concerned, it leaves aside the problem of absorption on the channel walls, allowing the flow to be studied separately from the absorption effect. Microdroplets can be generated within microfluidic devices using different methods such as electric fields,<sup>21</sup> microinjectors,<sup>22</sup> and needles.<sup>23</sup> However, the most widely used methods for the droplet generation rely on interfacial instabilities between immiscible fluids. Droplets are produced via snap-off or Rayleigh instability mechanisms by either T-junction or flow-focusing methods, respectively. A T-junction is a simple intersection of one fluid entering another stream at a  $90^\circ$  angle.<sup>24</sup> Thorsen demonstrated that varying disperse and continuous phase pressures in T-junctions yielded an array of fascinating structures.<sup>25</sup> Since then, many important aspects of fluid behavior have been elucidated by studying droplet breakup<sup>26,27</sup> and droplet manipulation,<sup>28,29</sup> using a T-junction setup. A flow-focusing design consists of a focusing fluid flanking or surrounding the core fluid so as to give rise to droplet or bubble break-off in the vicinity of an orifice through which both fluids are extruded.<sup>30,31</sup> Shelley Anna *et al.*<sup>30</sup> described two different droplet formation regimes in a flow-focusing design at the microfluidic systems. They studied the relationship between the size of the droplets formed and the ratio of flow rates between the dispersed phase and the continuous phase. Ward *et al.*<sup>31</sup> studied flow-focusing geometries and focused on the comparison between systems of droplet production driven by pressure and systems driven by flow rate. However, there are only a few studies at the mesoscale between the micro- and millifluidics using channels with diameters in the range over  $500\ \mu\text{m}$ . Working at this scale offers many advantages. From a practical point of view, microdroplets can be generated by using devices with mesoscale channels<sup>32</sup> over  $500\ \mu\text{m}$  to  $1\ \text{mm}$ , which allows the access to microscale benefits such as reduced reaction volumes, but using mesofluidics instead to microfluidic devices whose fabrication is simple, fast, and inexpensive. The phenomena involved in such a mesofluidic system cannot be entirely described without taking account of a description of the complete range of scales from the microfluidic level to the system level, as could be the case of a porous medium. Investigations in the mesoscale are largely lacking, and the present work will deal specifically with the scale length ranging from  $500\ \mu\text{m}$  to  $1\ \text{mm}$ .

In the present work, droplets were generated in a T-junction of circular cross-section channels with diameter

$850\ \mu\text{m}$ , and droplets over  $400\ \mu\text{m}$  in diameter were formed. The formation regimes and the controlling parameters such as flow rates and capillary number were investigated. The capillary film thickness was studied in order to describe and characterize the different behaviors. The film is formed between the drops and the channel wall. This analysis takes into account the size of the drop and the thickness of the residual film, at the scales studied. It is important to distinguish different droplet formation regimes, as well as to have control of the droplet dimensions based on the possible technical applications.

We present the mechanism of droplet breakup in Sec. II A and capillary film thickness in Sec. II B. In Sec. III, we give a description of the system used in our experiments. The experimental results are shown in Sec. IV. In this section, we show a study of the size of drops and the dependence of the residual film thickness on the capillary number. In Sec. V, we discuss the obtained results, and conclusions are shown in Sec. VI.

## II. MODELS

### A. Mechanism of droplet breakup

Different mechanisms of droplet breakup have been proposed. The analysis of breakup models has been related to different droplet formation regimes. According to experimental observation,<sup>25,33,34</sup> four regimes have been identified for droplet formation at a T-junction, namely, the squeezing, dripping, jetting regimes, and, in a recent work, Tarchichi *et al.*<sup>35</sup> presented a fourth droplet formation regime called balloon regime.

In an experimental and numerical approach<sup>34,36</sup> for the squeezing regime, Garstecki found that the breakup mechanism responds essentially to a buildup of pressure, which results from the blocking of the main channel by the dispersed phase. In this regime, the shear force is small, the droplets can enter the main channel and grow until the channel is almost blocked, as shown in simulations by Kashid<sup>37</sup> (for more details, see Refs. 34, 36, and 37). Remarkably, the interfacial forces do not drive the breakup in this regime, at least not up to the end of the stage.<sup>34</sup> In this description, the droplet volume does not depend strongly on the capillary number but on the flow rate ratio of two fluids. The relationship between droplet sizes and flow rate ratio, in the squeezing regime at the microfluidic systems,<sup>25,34,36,38–42</sup> is given by

$$\frac{L}{w_c} = 1 + \alpha \frac{Q_d}{Q_c}, \quad (1)$$

where  $L$  is the length of the droplet,  $w_c$  the channel width,  $Q_d$  and  $Q_c$  the flow rates of the dispersed and continuous phases, respectively (see Fig. 1), and  $\alpha$  is a fitting parameter with different values in several references.

Another mechanism of droplet breakup was proposed by Thorsen,<sup>25</sup> who suggested that the dynamics of droplet formation is dominated by the balance of tangential shear stresses and interfacial tension (i.e., the capillary number) as expected in unbounded shear flows, via an analogy to breakup processes in shear and extensional flows.<sup>43–45</sup> In this mechanism (shear-driven breakup), an estimation of the droplet volume can be obtained by balancing two effects: the viscous drag

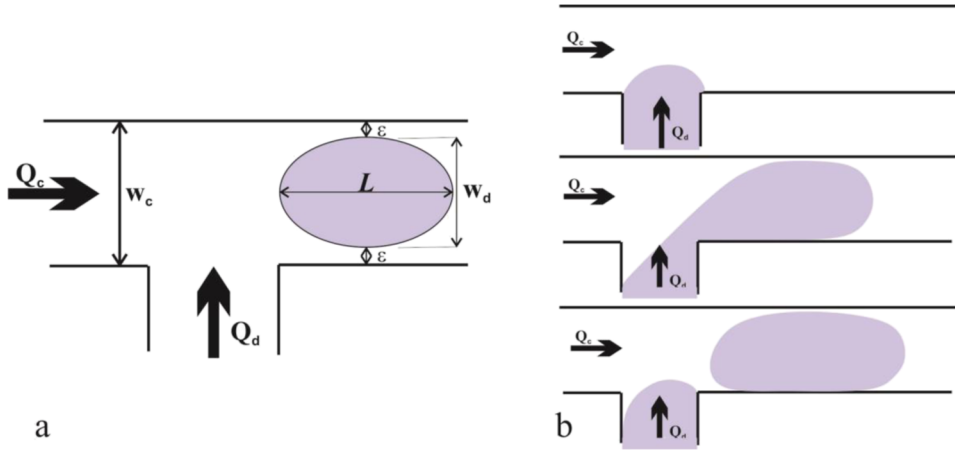


FIG. 1. (a) Diagram of the droplet formed in a T-junction experiment and notations used in the text. (b) Process of forming a drop.

applied on the emerging droplet by the continuous phase and the interfacial force opposite to the neck elongation connecting the reservoir of the dispersed fluid with the droplet.<sup>25,46</sup> The predicted size of a droplet under external shear force is then approximated by equating the Laplace pressure and the shear force,

$$\frac{L}{w_c} \propto \frac{1}{Ca}. \quad (2)$$

With this model, we obtain a relationship between the length of the droplet and the capillary number,  $Ca$ , calculated from  $Q_c$ ,<sup>47</sup>

$$Ca = \mu_c Q_c a^{-1} \sigma^{-1}, \quad (3)$$

where  $\mu_c$  is the viscosity of the continuous phase,  $\sigma$  is the interfacial tension between the dispersed and continuous phases, and  $a$  is the channel cross section. This definition of capillary number will be used throughout the work.

In an alternative approach, Van der Graff<sup>47</sup> assumed that the final droplet volume in a T-shaped microchannel is a result of two stages of droplet growth, namely, an expansion stage and a necking stage,

$$V_d = V_{\text{crit}} + t_{\text{neck}} Q_d, \quad (4)$$

where  $V_{\text{crit}}$  is the critical volume; it represents the volume at which the drag force exerted on the droplet is just as large as the interfacial tension-based force that attaches the droplet to the channel mouth, determined by a force or torque balance. This balance condition is similar to the Thorsen condition.  $t_{\text{neck}}$  is the time needed for necking;  $Q_d$  is the to-be-dispersed phase flow rate. By numerical and experimental analysis, Van der Graff arrives at a power law for  $V_{\text{crit}}$  and  $t_{\text{neck}}$ ; in this picture, the droplet volume dependence on the capillary number,  $V_d(Ca)$ , is given by

$$V_d = aCa^m + bCa^n Q_d. \quad (5)$$

In most cases,  $m = n$  is a good assumption, i.e., the droplet volume scales as  $Ca^n$ . Van der Graff found that  $V_d$  scales as  $Ca^{-0.75}$  and, therefore,  $L$  scales as  $Ca^{-0.25}$ .

## B. Capillary film thickness

The analysis of the lubrication film permits a better comprehension of the dynamics of the droplets propelled by an enfolding fluid in confined geometries. Landau and Levich<sup>48</sup>

were the first to determine theoretically the thickness of the film deposited by the withdrawal of a flat substrate from a bath of liquid with a clean interface. In the early 1960s, Bretherton studied the motion of an inviscid bubble in a cylindrical tube<sup>49</sup> and the influence of the lubrication film surrounding the bubble. The film has a uniform thickness,  $\epsilon$ , a long distance from the meniscus. This thickness,  $\epsilon$ , is related to the velocity of the bubble by means of a capillary number,  $Ca$ . In the regime where  $Ca \ll 1$ , the thickness of the film is

$$\epsilon_{\text{Breth}} = 1.34 r_c Ca^{2/3}, \quad (6)$$

where  $r$  is the radius of the channel,  $r_c = w_c/2$ .

Cachile *et al.*<sup>50</sup> reported a scaling law of the capillary film thickness, in a capillary tube of radius about 1 mm, resulting from the displacement of a fluid by an immiscible fluid. They studied the thickness average over the tube length, far from the meniscus tip, and reported

$$\epsilon_{\text{Cach}} \propto Ca^{0.6}. \quad (7)$$

Studying the inner and outer flow patterns of the droplet, Hodges *et al.*<sup>51</sup> derived a thickness correction:

$$\epsilon_{\text{Hod}} = \epsilon_{\text{Breth}} + \delta\epsilon_{\text{visc}} = A r_c Ca. \quad (8)$$

The prefactor  $A$  depends on the viscosity contrast between two fluids and verifies<sup>49</sup>  $A = 8.68$  for a droplet with a viscosity contrast  $\mu_d/\mu_c = 25$ . Recently, Huerre *et al.*<sup>52</sup> studied droplets of oil in water moving in a Hele-Shaw cell after being generated in a T-junction microfluidic system. They characterized two dynamical regimes of the film as a function of the capillary number,  $Ca < 10^{-4}$  (disjoining pressure-driven regime): the film thickness remains constant;  $Ca > 10^{-4}$  (viscosity-driven regime): the film thickness shows a quantitative agreement between the experimental data and theory for the viscous model proposed by Hodges *et al.* All of these studies were done without changing the droplet volume and in the same droplet formation regime, normally squeezing or dripping.

## III. EXPERIMENTAL SETUP

The system was built using polydimethylsiloxane (PDMS, Sylgard 184). The usual process to fabricate microfluidic devices includes soft lithography techniques, which generally involve the replication using a soft polymer

of a master structure etched on a photoresist plate. The methods are not adaptable to the mesoscale of interest to us because the photosensitive layers available commercially are too thin and they are not suitable for circular cross section. In the present work, the key idea is to implement a rapid prototyping easily adaptable to the mesoscale ( $500\ \mu\text{m}$  to  $1\ \text{mm}$  range) because the usual methods based on master molds in silicon wafers are not an option for such scales. Master molds built using rectified steel rods with  $850 \pm 5\ \mu\text{m}$  of diameter were used. The PDMS was poured on the rod master mold and put in a vacuum chamber to eliminate air bubbles. The PDMS was cured at  $80\ ^\circ\text{C}$  for 45 min. Finally, after peeling off the PDMS, the steel rods were extracted from the ends. The resulting T-junction channels have a circular cross section with a diameter of  $850\ \mu\text{m}$ .

Water (1 cP viscosity and 1 g/l density) and mineral oil (60 cP viscosity and 0.85 g/l density) were used at the continuous and dispersed phases, respectively. No surfactant was employed. Previously, in the present work, we studied these wetting properties prior to performing the droplet generation experiments. Mineral oil was chosen as continuous phase since it wets the PDMS surface more efficiently than water. As a result of the particular method to obtain the PDMS millifluidics chips, the PDMS surface was not treated with the plasma cleaning process commonly used in microfluidics. Two syringe pumps (Harvard Pump 22) were employed for injecting the dispersed phase and continuous phase flow, respectively, and the fluid was injected by homemade injectors placed at the ends of the channels and parallel to them.

Droplet formation at the T-junction was observed using a camera (Nikon D70) with its magnification increased by extension tubes. Images were recorded at full frame size, height: 3008 pixels, width: 2000 pixels. The droplet size was measured by counting pixels.

In order to remain close to technical applications, we mainly vary the flow of the continuous phase that is commonly used as a control fluid. In these applications, the dispersed phase is the fluid to be analyzed, and the continuous phase acts as dispersant and carrier. While the dispersed phase is limited by the amount of fluid available, there are fewer limitations for the choice and use of the continuous phase so that in many cases, it is interesting to study the behavior of the system as a function of the flow rates of the continuous phase.

#### IV. RESULTS

A typical process of droplet formation in the T-junction geometries was analyzed. Two immiscible fluids form an interface at the junction of two channels in T-type geometry. The stream of the dispersed phase from one of the channels penetrates into the other one, and a droplet begins to grow. When the interface approaches the downstream edge of the inlet for the dispersed phase, the neck connecting the inlet channel with the droplet breaks. The disconnected liquid plug flows downstream in the main channel, while the tip of the stream of the discontinuous phase retracts to the end of the inlet and the process repeats [see Fig. 1(b)].

Over a wide range of flow rates of both phases, this process generates uniformly sized droplets. The volume of these

droplets can be controlled by changing the flow rates of the dispersed phase and the carrier fluid. We chose the range of flow rates to obtain stable droplet formation regimes. Taking into account the channel sizes, fluids used and the nonuse of surfactants, for capillary numbers greater than those studied, the droplet formation process would be unstable and we would not obtain monodisperse droplet trains in that conditions.

Figure 2 show the images of droplets recorded at different flow rates of the continuous phase, with constant flow rate of the dispersed phase. These images exhibit two different regimes of droplet formation: squeezing and dripping. The squeezing regime is characterized by having elongated droplets that practically block the channel. Defining  $L$  as the length of the drop axis in the direction of the channel and  $w_d$ , the length of the axis in the direction transverse to it [see Fig. 1(a)], in the squeezing regime  $L > w_d$ ,  $L > w_c$ , and  $w_d \sim w_c$ . This confinement level determines the breakup mechanism of the drop, the dominant contribution to the dynamics of breakup arises from the buildup of pressure upstream of the emerging droplets Garstecki explains. In the dripping regime, the dimensions are  $L \sim w_d$  and  $L, w_d < w_c$ . Previous work<sup>34,36</sup> pointed out that the squeezing breakup mechanism is specific to the geometries used because it depends crucially on physical confinement of the interfacial dynamics. The analysis of the squeezing regime may be the key to understanding the transition of the micro- and macrofluidic behavior.

Figures 3 and 4 show plots of the dimensionless droplet length,  $L/w_c$  (see Fig. 1) as a function of, respectively, the flow rates  $Q_c$  and  $Q_d$  (the other flow rate being kept constant). The

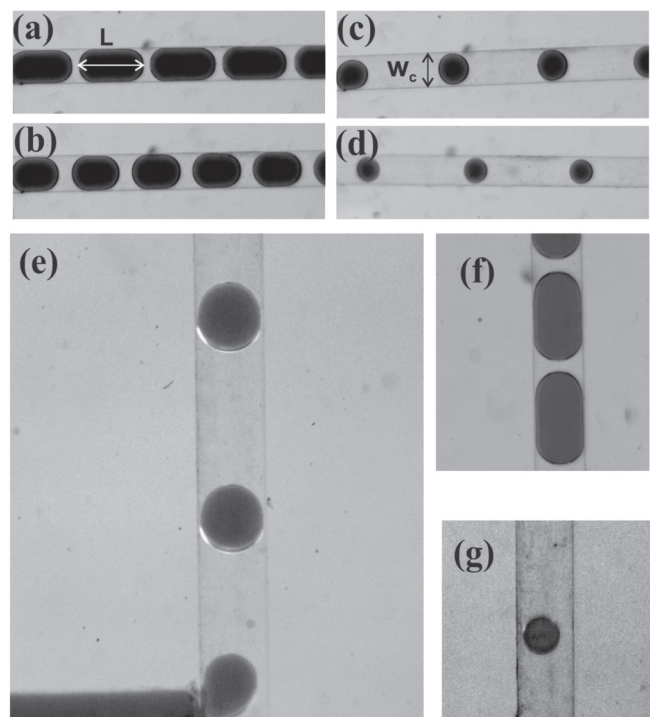


FIG. 2. Regimes of droplet formation,  $Q_d = 0.8\ \mu\text{l/s}$ . Squeezing regime: (a)  $Q_c = 0.5\ \mu\text{l/s}$ , (b)  $Q_c = 1.6\ \mu\text{l/s}$ . Dripping regime: (c)  $Q_c = 5\ \mu\text{l/s}$ , (d)  $Q_c = 7.5\ \mu\text{l/s}$ .  $L$ , Droplet length;  $w_c$ , channel width. (e) Detail of formation  $Q_c = 5\ \mu\text{l/s}$ , (f) largest droplet size  $Q_c = 0.16\ \mu\text{l/s}$ , (g) smallest droplet size  $Q_c = 10\ \mu\text{l/s}$ .

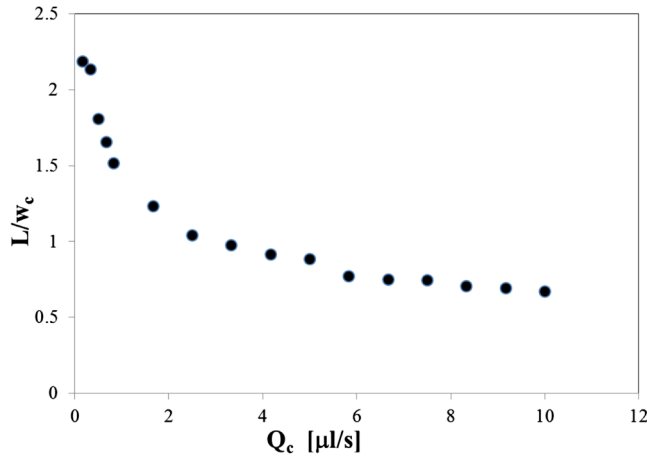


FIG. 3. Dimensionless droplet length ( $L/w_c$ ) vs. flow rate of continuous phase ( $Q_c$ ), flow rate of water ( $Q_d = 0.8 \mu\text{l/s}$ ). Errors: 3% for  $L/w_c$ , 1% for  $Q_c$ .

droplet breakup proceeds at a rate driven by the carrier flow rate, which sets the time for the growth of the droplet. As the carrier flow rate decreases, the time lapse until the breakup and, therefore, the volume of the droplets increase. We can observe this effect in Fig. 3. The flow rate of the dispersed phase, in turn, sets the final volume of the droplets reached at the time given by the carrier flow rate. The volume of droplets increases as the flow rate of the dispersed phase increases, as shown in Fig. 4.

The results shown in Figs. 3 and 4 are consistent with Eq. (1) proposed by Gartescki, but in order to analyze this dependence, a precise identification of droplet formation regimes is necessary. For this purpose, the experiments shown in Figs. 3 and 4 were performed: first, varying the continuous phase flow rate,  $Q_c$ , and leaving the flow rate of the dispersed phase,  $Q_d$ , fixed. Second, varying  $Q_d$  and fixing  $Q_c$ . In the first series of experiments, two regimes were observed: squeezing and dripping; in the second one, only the squeezing regime was observed.

### A. Size of droplets

The validity of the theoretical models at the mesoscale between the micro- and milliscale was tested. Figure 5

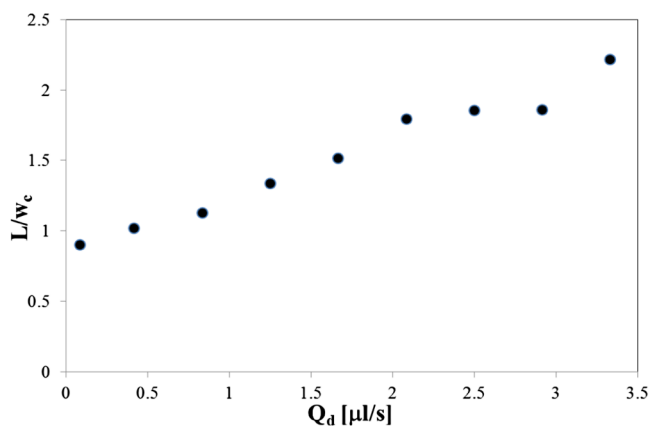


FIG. 4. Dimensionless droplet length ( $L/w_c$ ) vs. flow rate of dispersed phase ( $Q_d$ ), flow rate of continuous phase ( $Q_c = 0.8 \mu\text{l/s}$ ). Errors: 3% for  $L/w_c$ , 1% for  $Q_d$ .

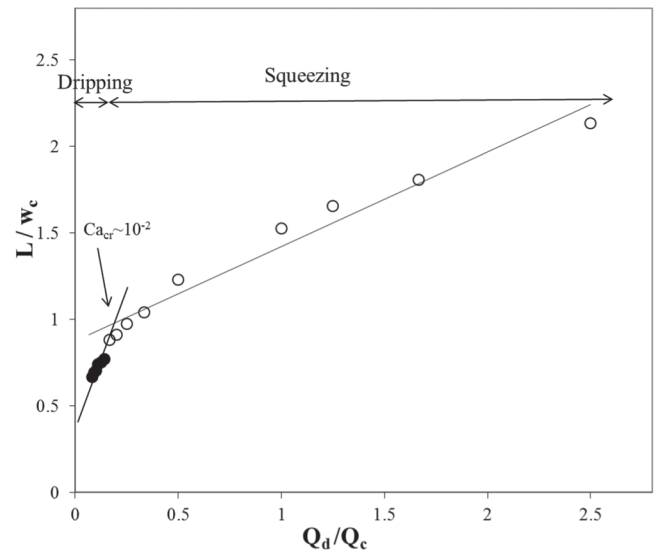


FIG. 5. Dimensionless droplet length ( $L/w_c$ ) vs. flow rate ratio ( $Q_d/Q_c$ ).  $\circ$ , Squeezing regime;  $\bullet$ , Dripping regime. Errors: 3% for  $L/w_c$ , 2% for  $Q_d/Q_c$ .

displays the dimensionless length of droplets ( $L/w_c$ ) vs. the flow rate ratio ( $Q_d/Q_c$ ). In the squeezing regime, Eq. (1) accurately fits the experimental data. However, the parameters for this fit by different authors are notably different, mainly because there are differences between the geometries considered. The occurrence of a squeezing regime even at the mesoscale is remarkable. This squeezing regime is well characterized by usual models independently of the capillary number; in contrast with the present experimental observations, models have been developed in highly confined geometries at the microscale. In Fig. 5, the experimental values corresponding to the squeezing and dripping regimes are distinguished (full circle, squeezing regime; empty circle, dripping regime). We consider, to this schematic differentiation, squeezing regime when the dimensions of the drops are such that  $L > w_d$  and  $w_d \sim w_c$  and dripping regime when  $L < w_c$  and  $L \sim w_d$ . A better determination of the regimen transition arises from the analysis of the results obtained. In Figs. 5–7, different variables of the same group of experiments are analyzed, so we will continue using the same markers styles to differentiate the two studied regimes.

Most previous studies have analyzed the regimes (dripping, squeezing, and jetting) separately; in most cases, these studies were centered in one regime observed. Particularly, in our work, the scaling law given by Eq. (1), where the dimensions of the formed droplets only depend on the flow rate ratio, fails to predict the behavior in the dripping regime. In the dripping regime,  $Ca$  plays a more important role than in the squeezing regime. On the other hand,  $Ca$  characterizes the transition between the regimes as discussed in Sec. III B.

Figure 6 shows the evolution of the droplet sizes as a function of the capillary number. In previous work at the microscale,<sup>36</sup> it was reported that the variation of  $L/w_c$  with  $Ca$  changes sharply from the squeezing to dripping regime. In the mesoscale system, the  $Ca_{cr}$  number that delimits the transition from one regime to the other is better defined by analyzing the residual film thickness curve or the slope changes of the  $L/w_c$  vs.  $Q_d/Q_c$  curve.

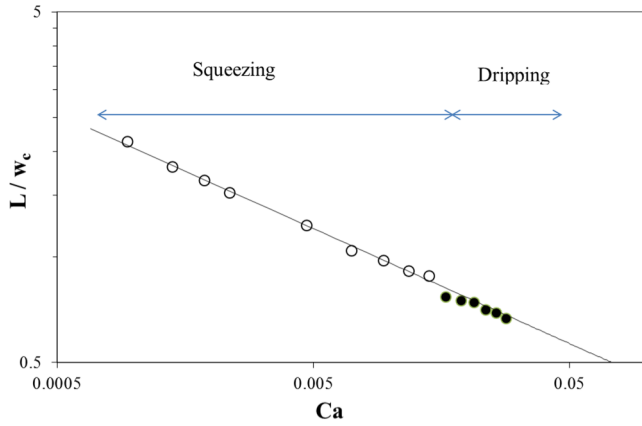


FIG. 6. Dimensionless droplet length ( $L/w_c$ ) vs. capillary number ( $Ca$ ).  $\circ$ , Squeezing regime;  $\bullet$ , Dripping regime. Errors: 1.5% for  $L$ , 3% for  $Ca$ .

At the microscale, the capillary film thickness typically remains below the tenth of a micrometer,<sup>52</sup> while at the mesoscale, the capillary film is in the range between  $25\ \mu\text{m}$  and  $50\ \mu\text{m}$  for the squeezing regime. At this scale, the influence of the viscous drag on the breakup mechanism becomes important. Therefore, a strong dependence of  $Ca$  even in the squeezing regime is observed as is shown in Fig. 6 and no sharp change in the droplet size is observed in the transition from squeezing to dripping. The experimental data were adjusted with the Van der Graaf model, which predicts a capillary number dependence of the droplet size, obtaining that  $L$  scales with  $Ca^{-0.32}$ , which is close to the data obtained by numerical approaches by Van der Graaf,<sup>46</sup>  $L \propto Ca^{-0.25}$ , and by De Menech,<sup>36</sup>  $L \propto Ca^{-0.4}$ .

## B. Capillary film thickness of confined droplets

The capillary film thickness,  $\varepsilon$ , is defined as the size of the space between the droplet contour and the channel inner wall, measured at the middle of the droplet (see Fig. 1). The behavior of this observable is linked to the evolution of droplet formation regimes.

Figure 7 shows the dependence of the capillary film thickness,  $\varepsilon$ , on the capillary number,  $Ca$ , for experiments where  $Q_c$  is varied. The capillary number was calculated in relation

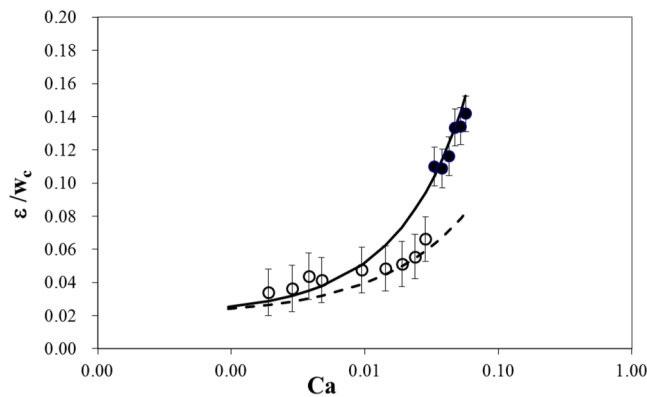


FIG. 7. Dimensionless capillary film thickness ( $\varepsilon/w_c$ ) vs. capillary number ( $Ca$ ).  $\bullet$ , Experimental data, dripping regime;  $\circ$ , Experimental data, squeezing regime. Solid line, the viscous model (Hodges); dashed line, the inviscid model (Bretherton). Errors: 3% for  $Ca$ .

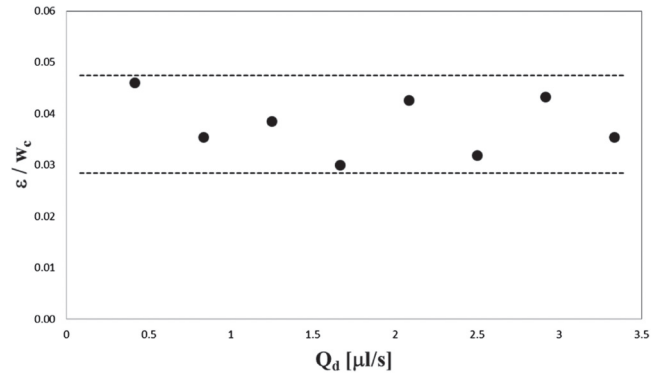


FIG. 8. Dimensionless capillary film thickness ( $\varepsilon/w_c$ ) vs.  $Q_d$ ; the capillary number remains constant.

to  $Q_c$ .<sup>47</sup> Data points in Figs. 5–7 correspond to the same 15 experiments.

Figure 7 shows that the capillary number reaches a critical value,  $Ca_{cr}$ . At this value of  $Ca$ , the system changes the operation regime, and  $Ca_{cr}$  defines the limit when the shear stress becomes so important that the regime switches to dripping. For  $Ca$  higher than  $Ca_{cr}$ , the capillary film thickness,  $\varepsilon$ , increases strongly and the droplet contour moves away from the inner walls. At values of  $Ca$  lower than  $Ca_{cr}$ , the values of  $\varepsilon$  grow slowly. In the mesoscale system,  $Ca_{cr}$  is  $\sim 10^{-2}$ , which is close to the critical value found in previous work at the microscale.<sup>34,36</sup> De Menech found a transition from the squeezing to the dripping regime at  $Ca \sim 1.5 \times 10^{-2}$  in numerical work by analyzing the volume of droplets as a function of  $Ca$ , and Garstecki confirmed these results in experimental work.

In Figure 7, the experimental data and the predictions of both the Bretherton inviscid model and the Hodges viscous model with  $\delta_{visc} = 5r_c Ca$  are plotted. The prefactor in  $\delta_{visc}$ , depending on the viscosity ratio  $\mu_c/\mu_d$ , was chosen to fit the experimental data. The power law of Bretherton underestimates the experimental results in the dripping regime and fits the squeezing regime quite precisely. Probably, the lower influence of viscosity in the squeezing regime<sup>34,36,39–42</sup> accounts for this behavior. The Hodges viscous model is in good agreement with experimental data, except for the transition from squeezing to dripping. At a low capillary number, both models converge and the viscous correction,  $\delta_{visc}$ , does not have a considerable weight. Near the critical value of  $Ca$ , but in the squeezing regime, the viscous model overestimates the experimental data, and the influence of viscosity becomes important in the dripping regime.

Figure 8 also shows the variation of  $\varepsilon$  with  $Q_d$ , in the experiments where  $Q_c$  remains constant. In this case, the capillary number still defined from Eq. (3) remains constant and  $\varepsilon$  does not depend on  $Q_d$ .

## V. DISCUSSION

The droplet formation process at a T-junction was studied experimentally at a meso-scale corresponding to the transition between micro- and milli-fluidics. We studied this process by a combined analysis of the breakup mechanisms and the lubrication film thickness. The effects of the control parameters,

including the flow rate and Ca number, were investigated in the squeezing and dripping droplet breakup regimes.

Results were compared to theoretical models and to results reported in micro-fluidic devices in the dripping and the squeezing regimes both observed in our experiments. Models taking into account the influence of the capillary number are necessary to account for the results obtained in both regimes, while the Garsteki model is only usable in the squeezing one. The analysis of the complete interval of measurements shows that the models with a capillary number dependence fit the experimental data quite precisely. In the less confined geometry, compared with the classical microfluidic geometries, droplets do not completely obstruct the cross section of the channel, even in the squeezing regime. In microfluidics, a typical channel of rectangular section,  $100\ \mu\text{m} \times 50\ \mu\text{m}$ , has an area of  $5 \times 10^3\ \mu\text{m}^2$ , while for the circular channels of diameter  $850\ \mu\text{m}$ , used here, area is  $5 \times 10^5\ \mu\text{m}^2$ . The effective section of the channel increases by two orders of magnitude and the fact that the capillary film increases by an order of magnitude makes the degree of confinement of the drops very different in each case. So in the physics of drop breakup, the effects of viscous drag and the effects of the abrupt change of pressure have different weights. We can calculate the degree of confinement by estimating the ratio between the capillary film thickness and the effective channel radius  $C_f = \varepsilon/w_{ef}$ , where  $\varepsilon$  is the thickness of the capillary film and  $w_{ef}$  is defined by  $\sqrt{A/\pi}$ ,  $A$  is the channel area. This definition coincides with the radius of the channel in the case of circular section channels. Therefore, we can see that  $C_f \sim 0$  in the case of very confined drops ( $\varepsilon \ll 1$ ) and  $C_f \sim 1$  in the case of slightly confined drops ( $\varepsilon \sim w_{ef}$ ). From the data measured by Huerre *et al.*,<sup>49</sup> we obtain a value for  $C_f \sim 10^{-2}$  ( $\varepsilon \sim 0.1\ \mu\text{m}$ ,  $w_{ef} \sim 12.5\ \mu\text{m}$ ) at the microscale and  $C_f \sim 10^{-1}$  ( $\varepsilon \sim 35\ \mu\text{m}$ ,  $w_{ef} \sim 425\ \mu\text{m}$ ) at the milliscale. We can see that  $C_f$  is an order of magnitude higher at the milliscale. Therefore, the viscous effects that modify the dynamics of the capillary film and the breakup mechanisms are larger at the millifluid scale than at the microfluidic scale.

The different regimes of droplet formation can be identified by studying the evolution of capillary film thickness. The critical capillary number, which marks the limit between the squeezing and dripping regimes, was determined. Two models have been discussed and compared to predict the variation of the capillary film thickness as a function of the capillary number. The Bretherton model, which does not take account of viscosity effects, fits the experimental data in the squeezing regime at low capillary numbers. In agreement with previous work, the effect of the dispersed phase viscosity in controlling the droplet diameter is more important in the dripping regime, while in the squeezing regime this influence is less important. A similar behavior can be expected for the capillary film thickness, and indeed the inviscid model of Bretherton precisely fits the data in that regime. As expected, in the dripping regime, the viscous effect is responsible for the difference between the experimental data and the Bretherton model; in this case, the model proposed by Hodge taking into account viscous effects is more accurate.

Based on the results obtained, we suggest that they might be transposed to the generation of droplets by a two phase

liquid-liquid flow through porous media. This mesofluidic study for models of porous media is of interest because, although not being as representative as an actual core sample, it provides *in situ* visualization of flow at the pore scale. Let us now consider a porous medium with pore sizes within the mesoscale with a pressure applied between the inlet and outlet of the sample. As is known, the pressure is uniform throughout the cross section to the flow; therefore, when applying the same pressure to channels of different diameters, we find different flow values. For miscible fluids, the geometry of drops increases the contact surface between different solutions and favors their mixing. If there are chemical reactions between the solutions, they would be favored by this effect. It is possible to amplify the difference between the flow rates with shear-thinning fluids, as demonstrated by D'Onofrio *et al.*<sup>53</sup> and Paterson *et al.*,<sup>1</sup> which would control the production of microdroplets and the squeezing or dripping regimes.

## VI. CONCLUSIONS

Our work reports original experiments complemented by a critical analysis and comparisons with several models from the literature and experimental results reported in channels of smaller sizes and generally different geometries. The combined analysis of the Bretherton and Hodge models shows that the role of the viscosity in different aspects of the squeezing regime is the key to understanding the passage from the millito the microscale. In droplet devices, the answer to when a system can be considered as a microfluidic system must be clarified in this analysis.

We showed a transition between two different droplet generations regimes (dripping and squeezing) when the capillary number based on the flow rate of the continuous phase is varied. This transition is particularly visible on the variation of the film thickness which can be quite well reproduced by theoretical models. The thickness varies instead, little with the flow rate of the dispersed phase. The same transition was also studied on the variation of the length of the drops with the same parameters and with the ratio of the flows of the two fluids.

We used channels with a circular cross-section that could eliminate some problems linked to channels with square or rectangular sections frequently used in microfluidics (influence of low velocity zones in the corners). We have developed a simple method for obtaining these channels. The connection of channels could simulate the inside of a porous medium. If inside a porous medium, the appropriate conditions for the formation of microdrops are given, it will be an effect to be taken into account when determining the dispersion produced by the porous medium. And if there are chemical reactions of the intervening solutions, the presence of drops increases the surface of contact between both of them and they will be favored.

## ACKNOWLEDGMENTS

We thank Eng. Guillermina Bertone for technical support. This work was financed by UBACYT program (Universidad de Buenos Aires, Argentina) and PIP program

(Consejo Nacional de Investigaciones Científicas y Técnicas, Argentina).

- <sup>1</sup>A. Paterson, A. D'Onofrio, C. Allain, J. P. Hulin, M. Rosen, and C. Gauthier, *J. Phys. II France* **6**, 1639 (1996).
- <sup>2</sup>A. D'Onofrio, A. Paterson, C. Allain, J. P. Hulin, and M. Rosen, in *Proceedings of the International Conference on Complex Colloidal Systems in Oil Industry* (Revue de l'Institut Français du Pétrole, 1997), Vol. 52, p. 219.
- <sup>3</sup>R. A. Wooding, *J. Fluid Mech.* **39**, 477 (1969).
- <sup>4</sup>R. A. Wooding, *Z. Angew. Math. Phys.* **13**, 255 (1962).
- <sup>5</sup>V. M. Freytes, A. D'Onofrio, M. Rosen, C. Allain, and J. P. Hulin, *Phys. A* **290**, 286 (2001), and references therein.
- <sup>6</sup>D. Fernández, L. Binda, A. Zalts, C. El Hasi, and A. D'Onofrio, *Chaos* **28**, 013108 (2018).
- <sup>7</sup>L. Binda, D. Fernandez, C. El Hasi, A. Zalts, and A. D'Onofrio, *Chaos* **28**, 013107 (2018).
- <sup>8</sup>M. Rosen, V. M. Freytes, A. D'Onofrio, C. A. Allain, and J. P. Hulin, *Granular Matter* **3**, 63–67 (2001).
- <sup>9</sup>C. Almarcha, P. M. J. Trevelyan, L. Riolfo, A. Zalts, C. El Hasi, A. D'Onofrio, and A. De Wit, *J. Phys. Chem. Lett.* **1**, 752 (2010).
- <sup>10</sup>S. Kuster, L. A. Riolfo, A. Zalts, C. El Hasi, C. Almarcha, P. M. J. Trevelyan, A. De Wit, and A. D'Onofrio, *Phys. Chem. Chem. Phys.* **13**, 17295 (2011).
- <sup>11</sup>A. Zalts, C. El Hasi, D. Rubio, A. Ureña, and A. D'Onofrio, *Phys. Rev. E* **77**, 015304(R) (2008).
- <sup>12</sup>G. García Casado, L. Tofaletti, D. Muller, and A. D'Onofrio, *J. Chem. Phys.* **126**, 114502 (2007).
- <sup>13</sup>D. Horváth, T. Banskí, Jr., and A. Toth, *J. Chem. Phys.* **117**, 4399 (2002).
- <sup>14</sup>J. Yang, A. D'Onofrio, S. Kalliadasis, and A. De Wit, *J. Chem. Phys.* **117**, 9395 (2002), and references therein.
- <sup>15</sup>D. Lima, A. D'Onofrio, and A. De Wit, *J. Chem. Phys.* **124**, 014509 (2006), and references therein.
- <sup>16</sup>R. Outeda, C. El Hasi, A. D'Onofrio, and A. Zalts, *Chaos* **24**, 013135 (2014).
- <sup>17</sup>C. Thomas, L. Lemaigre, A. Zalts, A. D'Onofrio, and A. De Wit, *Int. J. Greenhouse Gas Control* **42**, 525 (2015).
- <sup>18</sup>L. Macias, D. Müller, and A. D'Onofrio, *Phys. Rev. Lett.* **102**, 094501 (2009).
- <sup>19</sup>Y. Nagatsu, Y. Ishii, Y. Tada, and A. De Wit, *Phys. Rev. Lett.* **113**, 024502 (2014), and references therein.
- <sup>20</sup>L. Binda, C. El Hasi, A. Zalts, and A. D'Onofrio, *Chaos* **27**, 053111 (2017).
- <sup>21</sup>S. Kim, Y. Song, P. Skipper, and J. Han, *Anal. Chem.* **78**, 8011 (2006).
- <sup>22</sup>R. Lorenz, J. Edgar, G. Jeffries, and D. Chiu, *Anal. Chem.* **78**(18), 6433 (2006).
- <sup>23</sup>E. Quevedo, J. Steinbacher, and D. McQuade, *J. Am. Chem. Soc.* **127**(30), 10498 (2006).
- <sup>24</sup>W. L. Olbricht, *Annu. Rev. Fluid Mech.* **28**, 187 (1996).
- <sup>25</sup>T. Thorsen, R. W. Roberts, F. H. Arnold, and S. R. Quake, *Phys. Rev. Lett.* **86**, 4163 (2001).
- <sup>26</sup>J. D. Tice, H. Song, A. D. Lyon, and R. F. Ismagilov, *Langmuir* **19**, 9127 (2003).
- <sup>27</sup>J. D. Tice, A. D. Lyon, and R. F. Ismagilov, *Anal. Chim. Acta* **507**, 73 (2004).
- <sup>28</sup>H. Song, J. D. Tice, and R. F. Ismagilov, *Angew. Chem. Int. Ed.* **42**, 768 (2003).
- <sup>29</sup>B. Zheng, J. D. Tice, and R. F. Ismagilov, *Anal. Chem.* **76**, 4977 (2004).
- <sup>30</sup>Shelley L. Anna, Nathalie Bontoux, and Howard A. Stone, *Appl. Phys. Lett.* **82**, 364 (2003).
- <sup>31</sup>T. Ward, M. Faivre, M. Abkarian, and H. A. Stone, *Electrophoresis* **26**, 3716–3724 (2005).
- <sup>32</sup>J. L. Steinbacher, Y. Lui, B. P. Mason, W. L. Olbricht, and D. T. McQuade, *J. Flow Chem.* **2**, 56 (2012).
- <sup>33</sup>G. F. Christopher and S. L. Anna, *J. Phys. D: Appl. Phys.* **40**, 319 (2007).
- <sup>34</sup>P. Garstecki, M. J. Fuerstman, H. A. Stone, and G. M. Whitesides, *Lab Chip* **6**, 437 (2006).
- <sup>35</sup>N. Tarchichi, F. Chollet, and J. F. Manceau, *Microfluid. Nanofluid.* **14**, 45 (2013).
- <sup>36</sup>M. De Menech, P. Garstecki, F. Jousse, and H. A. Stone, *J. Fluid. Mech.* **595**, 141 (2008).
- <sup>37</sup>M. N. Kashid, A. Renken, and L. Kiwi-Minsker, *Chem. Eng. Res. Des.* **88**, 362 (2010).
- <sup>38</sup>T. Nisisako, T. Torii, and T. Higuchi, *Lab Chip* **2**, 24 (2002).
- <sup>39</sup>J. H. Xu, S. W. Li, J. Tan, Y. J. Wang, and G. S. Luo, *AIChE J.* **52**, 3005 (2006).
- <sup>40</sup>J. H. Xu, S. W. Li, J. Tan, and G. S. Luo, *Microfluid. Nanofluid.* **5**, 711 (2008).
- <sup>41</sup>H. H. Liu and Y. H. Zhang, *J. Appl. Phys.* **106**, 034906 (2009).
- <sup>42</sup>A. Gupta and R. Kumar, *Phys. Fluids* **22**, 122001 (2010).
- <sup>43</sup>G. I. Taylor, *Proc. R. Soc. Lond. A* **146**, 501 (1934).
- <sup>44</sup>J. M. Rallison, *Annu. Rev. Fluid Mech.* **16**, 45 (1984).
- <sup>45</sup>H. A. Stone, *Annu. Rev. Fluid Mech.* **26**, 65 (1994).
- <sup>46</sup>P. B. Umbanhowar, V. Prasad, and D. A. Weitz, *Langmuir* **16**, 347 (2000).
- <sup>47</sup>S. Van der Graff, T. Nisisako, C. Schroen, R. G. M. Van der Sman, and R. M. Boom, *Langmuir* **22**, 4144 (2006).
- <sup>48</sup>L. Landau and B. Levich, *Acta Physicochim. USSR* **7**, 42 (1942).
- <sup>49</sup>F. Bretherton, *J. Fluid Mech.* **10**, 166 (1961).
- <sup>50</sup>M. Cachile, R. Chertcoff, A. Calvo, M. Rosen, J. P. Hulin, and A. M. Cazabat, *J. Colloid Interface Sci.* **182**, 483 (1996).
- <sup>51</sup>S. R. Hodges, O. Jensen, and J. M. Rallison, *J. Fluid Mech.* **501**, 279 (2004).
- <sup>52</sup>A. Huerre, O. Theodoly, A. M. Leshansky, M. P. Valignat, I. Cantat, and M. C. Jullien, *Phys. Rev. Lett.* **115**, 064501 (2015).
- <sup>53</sup>A. D'Onofrio, V. M. Freytes, M. Rosen, C. Allain, and J. P. Hulin, *Eur. Phys. J. E* **7**, 251–259 (2002).